Structures 9 (2017) 21–28

Contents lists available at ScienceDirect

Structures

journal homepage: www.elsevier.com/locate/structures

Hot-Rolled Steel and Steel-Concrete Composite Design Incorporating Strain Hardening

L. Gardner, X. Yun *, L. Macorini, M. Kucukler

Department of Civil and Environmental Engineering, Imperial College London, South Kensington Campus, London, UK

ARTICLE INFO

Article history:
Received 28 April 2016
Received in revised form 29 July 2016
Accepted 7 August 2016
Available online 8 August 2016

Keywords:
Composite beams
Continuous strength method
Deformation based design
Hot-rolled steel
Steel structures

ABSTRACT

Current design codes for steel and steel-concrete composite structures are based on elastic, perfectly plastic material behaviour and can lead to overly conservative strength predictions due to the neglect of the beneficial influence of strain hardening, particularly in the case of stocky, bare steel cross-sections and composite beams under sagging bending moments. The Continuous Strength Method (CSM) is a deformation based design method that enables material strain hardening properties to be exploited, thus resulting in more accurate capacity predictions. In this paper, a strain hardening material model, which can closely represent the stress-strain response of hot-rolled steel, is introduced and incorporated into the CSM design framework. The CSM cross-section resistance functions, incorporating strain hardening, are derived for hot-rolled steel sections in compression and bending, as well as hot-rolled steel-concrete composite sections where their neutral axes lie within the concrete slab in bending. Comparisons of the capacity predictions with a range of experimental data from the literature and finite element data generated herein demonstrate the applicability and benefits of the proposed approach.

1. Introduction

The concept of cross-section classification is used in current design codes to determine the appropriate structural design resistance of metallic sections. The method limits the maximum stress in the cross-section to the yield stress f_y, neglecting the beneficial effects of strain hardening. Experimental results have shown that the current design methods, based on the idealised elastic, perfectly plastic material behaviour, are often conservative in estimating the resistance of stocky hot-rolled steel cross-sections in both compression and bending [1–3] and composite beams under sagging bending moments [4–6]. The Continuous Strength Method (CSM) is a newly developed deformation based approach to steel design that provides an alternative treatment to cross-section classification, and enables the effective utilization of strain hardening. The method was originally developed for stainless steel structural elements [7–9], which exhibit a high degree of strain hardening, and the same concept has since been applied to structural carbon steel [10–12] and aluminium alloy [13] design.

A bi-linear (elastic-linear hardening) material model has been employed in the CSM to date, providing consistency and a satisfactory representation for design purposes of the observed stress-strain responses of cold-formed steel, stainless steel and aluminium alloys [9, 12,13]. However, due to the existence of a yield plateau, this CSM bi-linear material model is less suitable for hot-rolled carbon steel. Thus, a revised CSM material model is proposed for hot-rolled carbon steel that exhibits a yield point, a yield plateau and a strain hardening region. In this paper, the application of the CSM to bare hot-rolled structural steel elements, focusing primarily on cross-sections in compression and bending, including recent developments and comparisons with test results, is outlined. Extension of the method to composite beams under sagging bending moments is then described.

2. Application of the CSM to hot-rolled steel elements

The key characteristics of the CSM lie in the employment of a base curve that defines the maximum level of strain ε_{csm} ε_{csm}that a cross-section can endure prior to failure by (inelastic) local buckling and the adoption of a material model that allows for strain hardening.

2.1. CSM design base curve

The CSM design base curve provides a continuous relationship between the strain ratio $\varepsilon_{csm}/\varepsilon_y$ and the cross-section slenderness $\overline{\lambda}_p$, where ε_y is the yield strain of the material equal to f_y/E, with f_y being the material yield strength and E being the Young's modulus. Within the CSM, the cross-section slenderness $\overline{\lambda}_p$ is defined in non-dimensional form as the square root of the ratio of the yield stress f_y to the elastic buckling stress σ_{cr}, as given by Eq. (1). The elastic buckling stress σ_{cr} should be determined for the full cross-section either using numerical methods, such as the finite strip software CUFSM [14], or approximate analytical methods [15]. As a conservative alternative, the elastic buckling stress of the full cross-section may be taken as that of

* Corresponding author.
E-mail address: x.yun14@imperial.ac.uk (X. Yun).

http://dx.doi.org/10.1016/j.istruc.2016.08.005
2352-0124/

its most slender element using the classical plate buckling expression [16]. The former approach considers plate element interaction effects within the cross-section, as used in the direct strength method [17], whereas the classical plate buckling expression assumes simply supported conditions at the edges of the adjoining plates, which neglects element interaction and generally results in a conservative prediction of σ_{cr}. More favourable results are obtained when the effects of plate element interaction are considered, and this is therefore recommended, and adopted in the analyses performed herein by calculating σ_{cr} using CUFSM [14]. The CSM design base curve is given by Eq. (2), where ε_u is the strain corresponding to the ultimate tensile stress f_u. Two upper bounds have been placed on the predicted cross-section deformation capacity $\varepsilon_{csm}/\varepsilon_y$; the first limit of 15 corresponds to the material ductility requirement expressed in EN 1993-1-1 [18] and prevents excessive deformations and the second limit of $C_1\varepsilon_u/\varepsilon_y$, where C_1 is a coefficient corresponding to the adopted CSM material model as described in the next section, defines a 'cut-off' strain to prevent over-predictions of material strength. It is noted that the CSM does not currently apply to cross-sections where $\overline{\lambda}_p$>0.68, which is the boundary between slender and non-slender sections [9], though developments are underway in this area.

$$\overline{\lambda}_p = \sqrt{f_y/\sigma_{cr}} \tag{1}$$

$$\frac{\varepsilon_{csm}}{\varepsilon_y} = \frac{0.25}{\overline{\lambda}_p^{3.6}} \text{ but } \frac{\varepsilon_{csm}}{\varepsilon_y} \le \min\left(15, \frac{C_1\varepsilon_u}{\varepsilon_y}\right) \tag{2}$$

2.2. Material model

An elastic, linear hardening material model has been adopted in the CSM to represent the strain hardening response of metallic materials, such as cold-formed steel, stainless steel and aluminium alloys. Despite the fact that the actual observed stress-strain response of these materials is rounded, the elastic, linear hardening CSM material model has been shown to capture the general strain hardening behaviour sufficiently well to enable accurate design capacity predictions [9,12,13]. However, this bi-linear material model is less suitable for hot-rolled carbon steel due to the presence of the characteristic yield plateau, with strain hardening not commencing until the attainment of the strain hardening strain ε_{sh}. Thus, a revised quad-linear material model, as illustrated in Fig. 1, is proposed for hot-rolled carbon steel considering both the length of the yield plateau and the strain hardening behaviour.

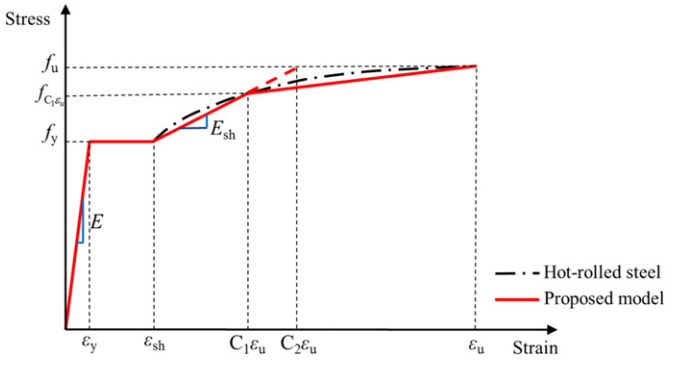

Fig. 1. Typical stress-strain curve for hot-rolled carbon steel and the proposed quad-linear material model.

The adopted stress-strain model consists of four stages and can be written over the full range of tensile strains as:

$$f(\varepsilon) = \begin{cases} E\varepsilon & \text{for } \varepsilon \le \varepsilon_y \\ f_y & \text{for } \varepsilon_y \le \varepsilon \le \varepsilon_{sh} \\ f_y + E_{sh}(\varepsilon - \varepsilon_{sh}) & \text{for } \varepsilon_{sh} \le \varepsilon \le C_1\varepsilon_u \\ f_{C_1\varepsilon_u} + \dfrac{f_u - f_{C_1\varepsilon_u}}{\varepsilon_u - C_1\varepsilon_u}(\varepsilon - C_1\varepsilon_u) & \text{for } C_1\varepsilon_u \le \varepsilon \le \varepsilon_u \end{cases} \tag{3}$$

in which $C_1\varepsilon_u$ represents the strain at the intersection point of the third stage of the model and the actual stress-strain curve, and $f_{C_1\varepsilon_u}$ is the corresponding stress, as shown in Fig. 1. Two material coefficients, C_1 and C_2, are used in the material model. C_1 represents the interaction point discussed previously and effectively defines a 'cut-off' strain to avoid over-predictions of material strength and is included in the base curve (Eq. (2)); C_2 is used in Eq. (4) to define the strain hardening slope E_{sh}.

$$E_{sh} = \frac{f_u - f_y}{C_2\varepsilon_u - \varepsilon_{sh}} \tag{4}$$

Coupon test data on hot-rolled carbon steels from a series of existing experimental programs [1,3,11,19–31] were collected and analyzed to establish predictive expressions for ε_u, ε_{sh} and the material coefficients C_1 and C_2.

For the strain at the ultimate tensile stress ε_u, a comparison between the collected test data and the predictive expression (Eq. (5)) is shown in Fig. 2. For hot-rolled carbon steels, ε_u decreases with increasing f_y/f_u initially, but once f_y/f_u is greater than a value of about 0.9 (normally for high strength steels), ε_u remains almost constant. The expression for ε_u provides good average predictions of the test data, with a mean ratio of the predicted to test values of ε_u being 0.96, and a moderate coefficient of variation (COV) of 0.25. Test data for high strength hot-rolled carbon steel are fairly scarce and more test data are required to further verify Eq. (5).

$$\varepsilon_u = \begin{cases} 0.6\left(1 - \dfrac{f_y}{f_u}\right) & \text{for } \dfrac{f_y}{f_u} \le 0.9 \\ 0.06 & \text{for } 0.9 < \dfrac{f_y}{f_u} \le 1 \end{cases} \tag{5}$$

The collected coupon test data for strain hardening strain ε_{sh} is plotted against the ratio of f_y/f_u in Fig. 3, together with the full cross-section tensile test data reported by Wang et al. [23] and Foster and Gardner

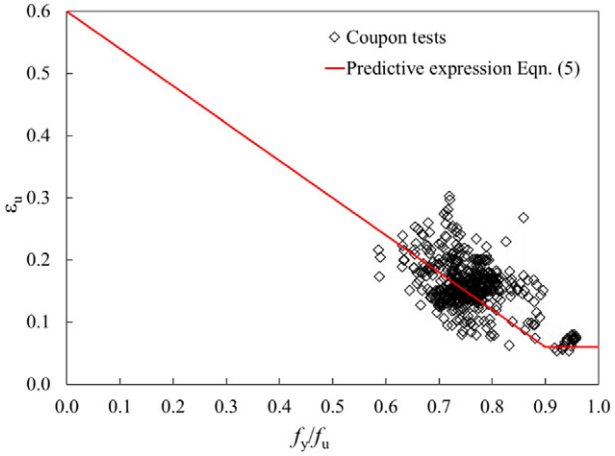

Fig. 2. Predictive expression for ε_u for hot-rolled carbon steels.

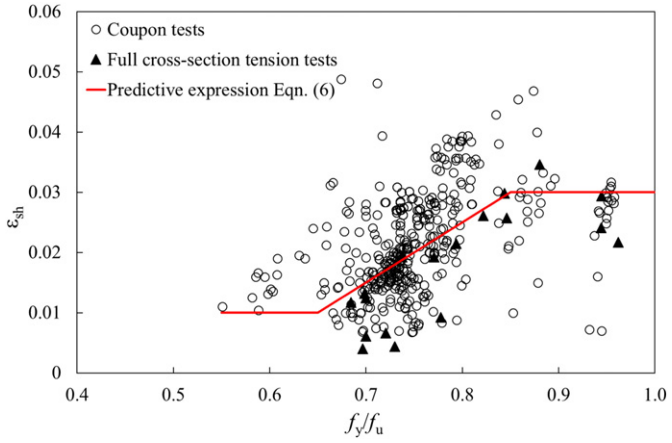

Fig. 3. Predictive expression for ε_{sh} for hot-rolled carbon steels.

[25]. Based on regression analysis, the following equation is proposed to predict ε_{sh} for hot-rolled carbon steels:

$$\varepsilon_{sh} = \begin{cases} 0.01 & \text{for } \frac{f_y}{f_u} \le 0.65 \\ 0.1\frac{f_y}{f_u} - 0.055 & \text{for } 0.65 < \frac{f_y}{f_u} \le 0.85 \\ 0.03 & \text{for } 0.85 < \frac{f_y}{f_u} \le 1 \end{cases} \quad (6)$$

Using the above equation, the mean value and COV for the ratios of predicted to test values of ε_{sh} are 1.05 and 0.42, respectively. Similarly, using least squares regression of the available experimental stress-strain curves on hot-rolled steel, the material coefficients C_1 and C_2 may be obtained from the following predictive expressions:

$$C_1 = \frac{\varepsilon_{sh} + 0.25(\varepsilon_u - \varepsilon_{sh})}{\varepsilon_u} \quad (7)$$

$$C_2 = \frac{\varepsilon_{sh} + 0.4(\varepsilon_u - \varepsilon_{sh})}{\varepsilon_u} \quad (8)$$

A detailed description of the quad-linear material model and its validation against further collected experimental stress-strain curves is currently being prepared.

2.3. Cross-section resistance

Within the CSM design framework, cross-section resistance is determined utilizing the strain ratio $\varepsilon_{csm}/\varepsilon_y$ from the design base curve (Eq. (2)), together with the adopted material model. In this paper, the quad-linear material model for hot-rolled steel, described in Section 2.2, is employed.

For non-slender cross-sections ($\overline{\lambda}_p \le 0.68$), the CSM axial compressive resistance $N_{csm,Rd}$ is calculated as the product of the gross cross-sectional area A and the CSM limiting material stress f_{csm}, as given by Eq. (9), in which γ_{M0} is a partial safety factor for cross-section resistance with a recommended value of unity for steel elements [18] and f_{csm} may be calculated from Eq. (10) based on the proposed material model. Note that only the second and third stages of the quad-linear model are used in the CSM, since currently the method applies to non-slender cross-sections ($\varepsilon_{csm}/\varepsilon_y \ge 1$), and progression into the fourth stage would correspond to very high strains and lead to overly complicated resistance functions, particularly in bending.

$$N_{csm,Rd} = \frac{A f_{csm}}{\gamma_{M0}} \quad (9)$$

$$f_{csm} = \begin{cases} f_y & \text{for } \varepsilon_y \le \varepsilon_{csm} \le \varepsilon_{sh} \\ f_y + E_{sh}(\varepsilon_{csm} - \varepsilon_{sh}) & \text{for } \varepsilon_{sh} < \varepsilon_{csm} \le C_1 \varepsilon_u \end{cases} \quad (10)$$

For sections with $\overline{\lambda}_p \le 0.68$, the cross-section resistance in bending $M_{csm,Rd}$ depends upon whether or not strain hardening is experienced (i.e. whether or not $\varepsilon_{csm} > \varepsilon_{sh}$). If $\varepsilon_{csm} \le \varepsilon_{sh}$, then the cross-section bending resistance $M_{csm,Rd}$ is given by Eqs. (11) and (12) for major and minor axis bending, respectively, where W_{pl} is the plastic section modulus, W_{el} is the elastic section modulus, y and z refer to the major and minor axes, respectively, and α is a dimensionless coefficient that depends on the type of section and axis of bending as defined in Table 1. These expressions allow for the increasing resistance with increasing deformation capacity (i.e. strain ratio $\varepsilon_{csm}/\varepsilon_y$) due to the spread of plasticity.

$$M_{y,csm,Rd} = \frac{W_{pl,y} f_y}{\gamma_{M0}} \left[1 - \left(1 - \frac{W_{el,y}}{W_{pl,y}} \right) \Big/ \left(\frac{\varepsilon_{csm}}{\varepsilon_y} \right)^{\alpha} \right] \quad \text{for } \varepsilon_{csm} \le \varepsilon_{sh} \quad (11)$$

$$M_{z,csm,Rd} = \frac{W_{pl,z} f_y}{\gamma_{M0}} \left[1 - \left(1 - \frac{W_{el,z}}{W_{pl,z}} \right) \Big/ \left(\frac{\varepsilon_{csm}}{\varepsilon_y} \right)^{\alpha} \right] \quad \text{for } \varepsilon_{csm} \le \varepsilon_{sh} \quad (12)$$

For the more stocky cross-sections, where $\varepsilon_{csm} > \varepsilon_{sh}$, some benefit from strain hardening can also be exploited, and the CSM cross-section bending resistance is given by Eqs. (13) and (14), for major axis and minor axis bending, respectively, where β is a dimensionless coefficient, values of which are given in Table 1.

$$M_{y,csm,Rd} = \frac{W_{pl,y} f_y}{\gamma_{M0}} \left[1 - \left(1 - \frac{W_{el,y}}{W_{pl,y}} \right) \Big/ \left(\frac{\varepsilon_{csm}}{\varepsilon_y} \right)^{\alpha} + \beta \left(\frac{\varepsilon_{csm} - \varepsilon_{sh}}{\varepsilon_y} \right)^2 \frac{E_{sh}}{E} \right] \quad \text{for } \varepsilon_{csm} > \varepsilon_{sh} \quad (13)$$

$$M_{z,csm,Rd} = \frac{W_{pl,z} f_y}{\gamma_{M0}} \left[1 - \left(1 - \frac{W_{el,z}}{W_{pl,z}} \right) \Big/ \left(\frac{\varepsilon_{csm}}{\varepsilon_y} \right)^{\alpha} + \beta \left(\frac{\varepsilon_{csm} - \varepsilon_{sh}}{\varepsilon_y} \right)^2 \frac{E_{sh}}{E} \right] \quad \text{for } \varepsilon_{csm} > \varepsilon_{sh} \quad (14)$$

2.4. Comparison with test data and design methods

The resulting predictions from the CSM have been compared with experimental data on 20 hot-rolled carbon steel stub columns [1,2,11] and 97 beams [1,3,11,32–35]. All comparisons are made on the basis of the measured geometric and material properties and with all partial factors set equal to unity. The average ratios of ultimate test loads N_{test} and moments M_{test} to the CSM (N_{csm}, M_{csm}) and EN 1993-1-1 (N_{EC}, M_{EC}) predicted resistances have been determined and are summarized in Table 2. The coefficients of variation (COV) have also been calculated to quantify the scatter of the predictions, and are presented in Table 2. It can be seen that the CSM provides more accurate and consistent predictions compared with those from EN 1993-1-1 [18], especially in the bending predictions for the Class 3 cross-sections where an average of 9% enhancement in capacity can be obtained using the CSM due to its accurate consideration of the spread of plasticity. Further research is currently underway into refining the material model, incorporating a larger pool of data on hot-rolled carbon steel material and cross-sections, and reliability analysis.

Table 1
CSM coefficients α and β for use in bending resistance functions.

Axis of bending	α		β	
	Major	Minor	Major	Minor
I-sections	2	1.2	0.1	0.05
SHS/RHS	2	2	0.1	0.1

Table 2
Comparison between ultimate test capacities and design (CSM and EC3) predictions for cross-section in compression or bending.

	Compression resistance		Bending resistance			
	N_{test}/N_{EC}	N_{test}/N_{csm}	M_{test}/M_{EC}		M_{test}/M_{csm}	
			Class 1 & 2	Class 3	Class 1 & 2	Class 3
Mean	1.07	1.06	1.18	1.17	1.16	1.08
COV	0.08	0.07	0.10	0.10	0.09	0.08

3. Application of the CSM to composite beams

3.1. Background

Steel-concrete composite construction seeks to harness the combined merits of the two materials to enable more efficient and economical structural solutions. The case of simply supported composite beams under sagging bending moment, whereby the concrete is largely in compression and the steel in tension, offers the greatest opportunity to exploit the full capacity of both materials. Composite beams having a ductile cross-section, defined as one in which the geometrical and material properties are such that strain hardening of the lower flange occurs before the collapse moment is reached, are desirable in engineering applications since the full plastic moment capacity can be utilized. Current design codes for composite structures, including EN 1994-1-1 [36], employ simple rigid plastic analysis to calculate the cross-section bending capacity of composite beams and, as for the design of bare steel beams, strain hardening effects in the steel are usually neglected. This can be rather conservative, as shown in several experimental and numerical studies [4,6], where substantial benefits from strain hardening have been observed. Note that the influence of strain hardening is implicitly included in the determination of the minimum degree of shear connection required to achieve the plastic bending resistance of composite beams in Eurocode 4 [37], but increases in load-bearing capacity for beams with full shear connection, beyond those derived from rigid-plastic theory, are not accounted for.

The focus of this section of the paper is on the assessment of Eurocode 4 and the development of a more efficient method for the design of composite beams under sagging bending moment, based on the results of existing experiments and numerical simulations. An analytical model is developed to calculate the bending capacity of composite beams with full shear connection, allowing for the influence of strain hardening through the quad-linear material model introduced in Section 2.2. Comparisons of the resistances obtained from the proposed design expressions with test results are made to demonstrate the accuracy and benefits of the method. Finally, a two-dimensional finite element (FE) model is established and validated against experimental results reported elsewhere. Upon validation of the FE models, parametric studies are performed to investigate the response of composite beams with partial shear connection, considering the effects of the steel grade and degree of partial shear connection. An indicative design approach is then proposed.

3.2. Full shear connection

In the case of composite beams with full shear connection, where the shear connection deformability is small, a single neutral axis exists and the bending resistance can be derived analytically using simple equilibrium considerations in conjunction with suitable material laws. Herein, an analytical expression for the bending resistance, incorporating strain hardening, is derived for one scenario, that being where the neutral axis lies within the concrete. For other scenarios where the neutral axis lies within the steel cross-section, expressions for bending resistance have been derived by Kucukler [38], though benefit from strain hardening is less likely to be achieved with the presented material model. The analytical model developed in this paper is based on the following assumptions:

- The slip between the steel section and concrete slab is ignored and the distribution of strains throughout the depth of the cross-section is linear, with constant curvature κ, as shown in Fig. 4.
- The composite beam has a ductile cross-section, with its neutral axis lying within the concrete slab and the strain at the bottom outer fibre of the steel section reaching ε_{sh}, as shown in Fig. 4, which requires $y_{csm}/(h_c + h_a) \le \varepsilon_{c,csm} / (\varepsilon_{c,csm} + \varepsilon_{sh})$, where y_{csm} is the distance between the plastic neutral axis and the extreme fibre of the concrete slab in compression, h_c is the depth of the concrete slab, h_a is the depth of the steel section and $\varepsilon_{c,csm}$ is the outer fibre concrete strain.
- The stress-strain relationship for the structural steel is represented by the quad-linear material response of Fig. 1, while the concrete material behaviour is assumed to be rigid plastic, with plasticity occurring at a stress level of $0.85f_{cd}$, where f_{cd} is the design concrete (cylinder) compressive strength. The tensile strength of the concrete is ignored.
- The stress within the bottom flange of the steel section is assumed to be constant through the plate thickness, and the stress $f_{csm,a}$ is determined using the strain at its mid-thickness $\varepsilon_{a,csm}$.
- The presence of any reinforcement in the slab is ignored.

For composite beams with full shear connection under sagging bending moments, deformation capacity will typically be limited by either crushing of the concrete slab or the tensile ductility of the structural steel. In this study, the maximum outer fibre concrete strain is limited by the crushing strain of the concrete ε_{cu} (i.e. $\varepsilon_{c,csm} = \varepsilon_{cu} = 0.0035$), while the maximum outer fibre strain (at the mid-thickness of the bottom flange) in the steel $\varepsilon_{a,csm}$ has been limited to $15\varepsilon_y$.

The initial step in the determination of the bending resistance is to locate the position of the neutral axis at failure. However, the neutral axis shifts under increasing curvature, and its location at failure will therefore depend on which of the two failure modes (concrete or steel) governs. The general relationship, calculated from the equilibrium of internal forces, between curvature κ_{csm} and neutral axis position y_{csm} is given by Eq. (15), in which b_{eff} is the effective width of the concrete slab, A_a is the cross-sectional area of the steel section, t_w is the web thickness of the steel beam and b_f and t_f are the flange width and thickness of the steel beam, respectively.

$$0.85f_{cd}b_{eff}y_{csm} = f_yA_a + \left(f_{csm,a} - f_y\right)b_ft_f + 0.5t_w\left(f_{csm,a} - f_y\right)\left(h_c + h_a - y_{csm} - \frac{\varepsilon_{sh}}{\kappa_{csm}}\right) \quad (15)$$

Based on the governing values of κ_{csm} and y_{csm} and the proposed material model (Fig. 1), the outer fibre stresses in the steel section at failure can be determined from Eq. (16).

$$f_{csm,\ a} = f_y + E_{sh}[\kappa_{csm}(h_c + h_a - y_{csm}) - \varepsilon_{sh}] \quad (16)$$

For the case where concrete crushing governs, the limiting curvature $\kappa_{csm,c}$ for concrete failure can be determined from Eq. (17), representing the limiting strain of concrete ε_{cu} being reached at the outer concrete fibre.

$$\kappa_{csm,c} = \frac{\varepsilon_{cu}}{y_{csm}} = \frac{0.0035}{y_{csm}} \quad (17)$$

Substituting Eqs. (16) and (17) into Eq. (15), the quadratic Eq. (18) can be derived to determine the position of the neutral axis $y_{csm,c}$, in which the coefficients B, C and D are given by Eqs. (19), (20) and (21), respectively.

$$By_{csm,c}^2 + Cy_{csm,c} + D = 0 \quad (18)$$

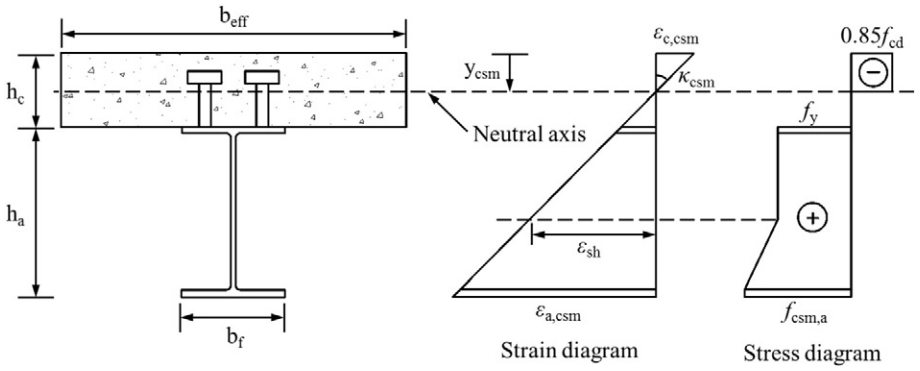

Fig. 4. Strain and stress distributions for a composite beam with full shear connection and the proposed material model.

$$B = 0.85 f_{cd} b_{eff} - \frac{0.0035}{2} t_w E_{sh} \left(1 + \frac{\varepsilon_{sh}}{0.0035}\right)^2 \quad (19)$$

$$C = 0.0035 E_{sh} \left(1 + \frac{\varepsilon_{sh}}{0.0035}\right) [b_f t_f + t_w (h_c + h_a)] - f_y A_a \quad (20)$$

$$D = -0.0035 E_{sh} (h_c + h_a) \left[b_f t_f + \frac{t_w}{2} (h_c + h_a)\right] \quad (21)$$

When steel failure governs the deformation capacity (i.e. when the strain at the outer steel fibre reaches the limiting strain of $15\varepsilon_y$), the limiting curvature $\kappa_{csm,a}$ can be determined from Eq. (22):

$$\kappa_{csm,a} = \frac{15\varepsilon_y}{h_c + h_a - y_{csm,a}} \quad (22)$$

Similarly, substituting Eqs. (16) and (22) into Eq. (15) results in Eq. (23), which can be used to determine the neutral axis position $y_{csm,a}$ at the point of failure in the steel section.

$$y_{csm,a} = [f_y A_a + E_{sh}(15\varepsilon_y - \varepsilon_{sh}) b_f t_f + \frac{E_{sh}}{2}(15\varepsilon_y - \varepsilon_{sh}) t_w (h_c + h_a)\left(1 - \frac{\varepsilon_{sh}}{15\varepsilon_y}\right)] / \left[0.85 f_{cd} b_{eff} + \frac{E_{sh}}{2}(15\varepsilon_y - \varepsilon_{sh}) t_w \left(1 - \frac{\varepsilon_{sh}}{15\varepsilon_y}\right)\right] \quad (23)$$

The lower of $\kappa_{csm,c}$ and $\kappa_{csm,a}$ defines the governing failure mode. The relationship between the neutral axis position y_{csm} and its corresponding curvature κ_{csm} for a typical composite beam, given by Eq. (15), is plotted in Fig. 5 as an example to illustrate the above calculation process. The geometric and material properties employed are: b_{eff} = 1500 mm, h_c = 120 mm, f_{cd} = 35 N/mm^2, f_y = 355 N/mm^2, E = 210,000 N/mm^2 and the steel section is a UB 475 × 152 × 60. The strain hardening strain ε_{sh} and modulus E_{sh} were determined from Eqs. (6) and (4), respectively. In this case, at failure, the neutral axis position lies within the concrete slab and the steel section is fully yielded. Fig. 5 shows how the position of the neutral axis moves downwards with increasing curvature, and there is a change in slope as the deformation progresses through the elastic region, outer fibre yielding of the steel and strain hardening of the steel. The points at which the concrete failure criterion (Eq. (17)) and the steel failure criterion (Eq. (22)) intersect with Eq. (15) define the corresponding neutral axis positions and curvatures at failure. For the case illustrated, steel failure is the governing mode.

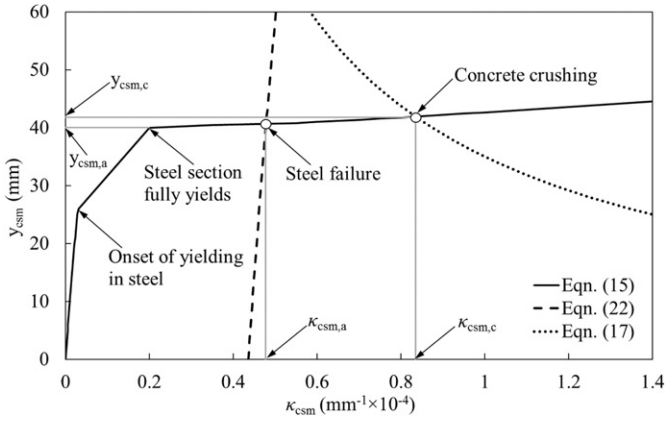

Fig. 5. Relationship between neutral axis position y_{csm} and curvature κ_{csm}.

Finally, the moment capacity of the composite section, considering the first three stages of the quad-linear material model, featuring both the yield plateau and strain hardening, can be calculated from Eq. (24).

$$M_{csm,c} = \left(f_{csm} - f_y\right) b_f t_f \left(h_c + h_a - \frac{y_{csm}}{2}\right) + f_y A_a \left(h_c + \frac{h_a}{2} - \frac{y_{csm}}{2}\right) + \frac{t_w}{12}\left(f_{csm} - f_y\right)\left(h_c + h_a - \frac{\varepsilon_{sh}}{\kappa_{csm}} - y_{csm}\right)\left[4(h_c + h_a) + 2\frac{\varepsilon_{sh}}{\kappa_{csm}} - y_{csm}\right] \quad (24)$$

The resistances obtained from the proposed analytical method have been compared against a series of experimental results collected from the literature [4,6] on composite beams with full shear connection. The comparisons, shown in Table 3, have been made on the basis of the measured geometric and material properties, with all partial factors set to unity. The proposed method, accounting for strain hardening, may be seen to provide a more accurate prediction of test capacity than the current approach given in Eurocode 4.

3.3. Partial shear connection

In the case of composite beams with partial shear connection, the contribution of strain hardening to the cross-section moment capacity cannot be calculated using the analytical method described in Section 3.2. The deformability and finite resistance of the shear connection leads to a more complex arrangement of internal forces in the composite section, with two distinct neutral axes lying within the concrete slab and the steel section. A numerical approach, using the finite element (FE) package ABAQUS [39], was adopted herein to predict the collapse load of composite beams with partial shear connection. The numerical models were initially validated against a series of

Table 3
Comparison between ultimate test moment capacities and design predictions (CSM and EC4) for composite beams.

	M_{EC}/M_{test}	$M_{csm,c}/M_{test}$	$M_{csm,c}/M_{EC}$
Mean	0.92	0.97	1.05
COV	0.05	0.06	–

experimental results and then used to perform parametric studies to generate additional data over a range of steel grades and shear connection ratios.

3.3.1. FE model and validation

The FE method has been used in a number of studies to investigate the behaviour of composite beams [40–43]. Among the previous research, a two-dimensional FE model for composite beams has been developed and validated by Queiroz et al. [42]. This two-dimensional model was shown to provide accurate results and was far more efficient than equivalent three-dimensional representations in terms of reduced numerical convergence issues and processing times. A similar approach was adopted in this paper. Geometric and material nonlinearities were considered in the model. The steel beam and concrete slab were modelled using quadratic beam elements (B22), while the mechanical shear connectors were simulated using rigid links (CONN2D2) and nonlinear spring elements (SPRINGA), as shown in Fig. 6.

The material properties of the steel beam were represented using the stress-strain curve shown in Fig. 1. In the validation of the two-dimensional FE models against existing tests, the steel reinforcement in the concrete slab was simulated using the *REBAR keyword in ABAQUS, which can be used to add discrete axial reinforcement to beam elements. Note that only longitudinal reinforcement was considered in the FE models for simplicity. An elastic perfectly plastic material model was used for the reinforcement. The nonlinear stress-strain relationship of concrete in compression was described using Eq. (25), according to EN 1992–1-1 (2004) [44] as:

$$\sigma_c/f_{cm} = \frac{k(\varepsilon_c/\varepsilon_{cl}) - (\varepsilon_c/\varepsilon_{cl})^2}{1 + (k-2)(\varepsilon_c/\varepsilon_{cl})} \quad (25)$$

where σ_c is the compressive stress (in MPa), f_{cm} is mean value of concrete cylinder compressive strength (in MPa), ε_c is the compressive strain, ε_{cl} is the compressive strain at the peak stress f_{cm} and taken as $\varepsilon_{cl} = \min(0.7f_{cm}^{0.31}, 2.8)‰$, $k = 1.05E_{cm}\varepsilon_{cl}/f_{cm}$, where the mean value of the secant modulus of elasticity of concrete E_{cm} (in GPa) is obtained from $E_{cm} = 22 \times (f_{cm}/10)^{0.3}$, ε_{cul} is the ultimate compressive strain and is taken as $\varepsilon_{cul} = \min[2.8 + 27 \times (98 - f_{cm}/100)^4, 3.5]‰$, and f_{ctm} is the mean value of the axial tensile strength (in MPa) and may be determined through $f_{ctm} = 0.3 \times (f_{cm} - 8)^{2/3}$ when $f_{cm} \le 58$ MPa, otherwise $f_{ctm} = 2.12 \times \ln(1 + f_{cm}/10)$. The concrete strain at cracking is taken as 0.01, beyond which the concrete carries zero stress. The stress-strain model for the concrete is illustrated in Fig. 7.

The approach taken to the modelling of the shear connectors is indicated in Fig. 6. The load-slip relationship proposed by Johnson and Molenstra [37] was used to simulate the shear stud connectors, where curve A and a maximum slip $s_{max} = 6$ mm was adopted in the present study. Failure was signified when the designated maximum strains in either of the materials were reached: $\varepsilon_{cul} = 0.0035$ for the concrete and $\varepsilon_{a,csm} = 15\varepsilon_y$ for the steel, or when the maximum allowable slip in the shear connectors, defined as $s_{max} = 6$ mm, was reached. The Riks solution method was used to trace the nonlinear equilibrium paths of the models and to obtain the peak loading magnitude.

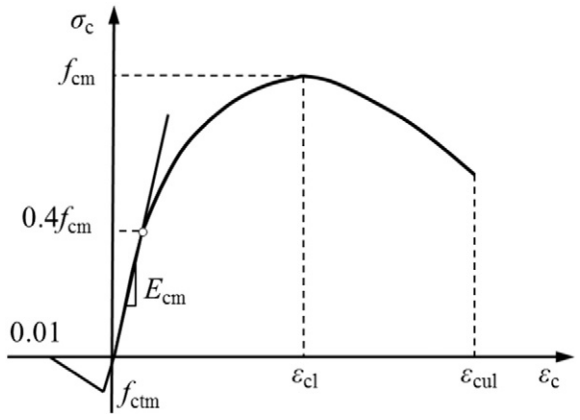

Fig. 7. Stress-strain relationship of concrete material employed in the FE model.

The FE model developed in this sub-section was employed to analyze a series of simply supported composite beams reported in the literature [4,5,45,46]. Experimental investigations with a total of 14 composite beams with full shear connection and 5 with partial shear connection were employed herein to validate the FE model. Two typical load versus mid-span deflection curves obtained from the FE model are compared with those obtained experimentally and numerically with a 3D FE model [43], as shown in Fig. 8.

The results indicate that the FE models developed herein are capable of accurately simulating the load-deformation response and ultimate capacity of composite beams with both full shear connection and partial shear connection, with the mean value of the ratio of FE ultimate capacity to test ultimate capacity (N_{FE}/N_{test}) being 0.99 and the COV being 0.054.

3.3.2. Parametric analysis and design approach

To evaluate the influence of the steel grade and the degree of shear connection η, which is defined as the ratio of the design value of the compressive normal force within the concrete flange N_c to the design value of the compressive normal force within the concrete flange with full shear connection $N_{c,f}$, 36 simply supported composite beams loaded by a point load at mid-span were analyzed using the validated FE model. Note that the occurrence of strain hardening is dependent on the neutral axis location and for higher degrees of shear connection, strain hardening was more prevalent, while for lower degrees of shear connection, failure by concrete crushing or shear stud ductility often prevented strain hardening from being achieved. The considered steel grades were S275, S355, S420 and S460, and the degrees of shear connection η ranged from 0.4 to 1.2. The beam cross-section dimensions (UB305 × 165 × 40) and the span length of 6 m were kept constant, while different steel grades, concrete slabs and grades and levels of shear connections were considered. The basic material parameters

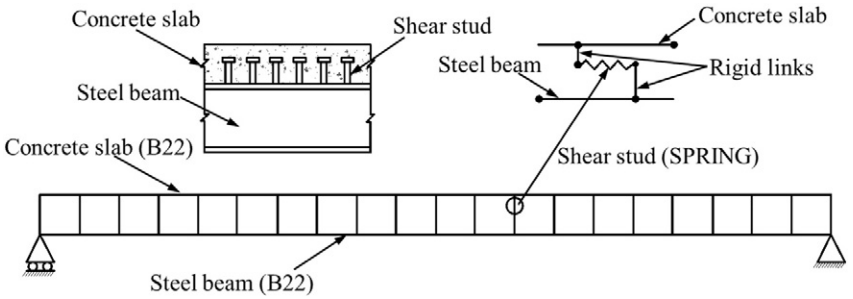

Fig. 6. Finite element types used in composite beam model.

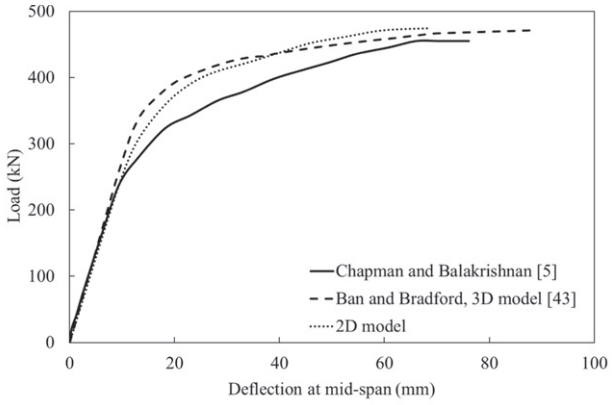

(a) Composite beam A5 with full shear connection

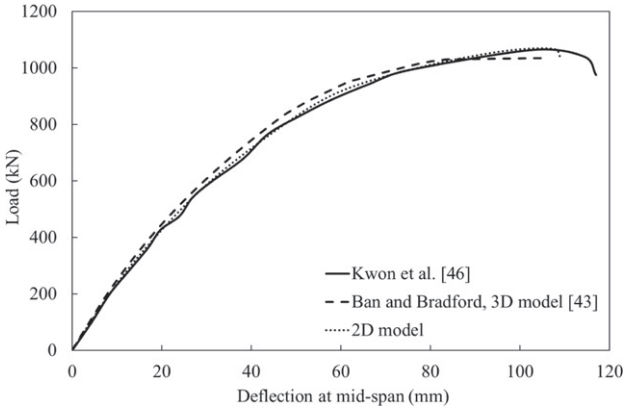

(b) Composite beam HASAA-30BS with partial shear connection

Fig. 8. Comparison of load-deflection curves from FE models and experiments.

and dimensions of the concrete slab are summarized in Table 4. The material models introduced into the FE model are determined according to the proposed equations described in sub-Section 2.2 for the steel and to Eurocode 2 for the concrete. The shear connectors were located uniformly along the entire span of the composite beams and their ultimate shear capacity was taken as 119 kN [5]. In the parametric studies, the number of the shear connectors was determined based on the prescribed values of η and the computed values of $N_{c,f}$. The reinforcement was not considered in the parametric studies; hence conservative predicted capacities may be obtained. Note that the amount of reinforcement provided can have a significant influence on composite beam behaviour [47], in terms of both the ductility and strength, and the reinforcement should be considered in future studies.

Eurocode 4 provides two alternative approaches, namely the equilibrium and the interpolation method, for the design of composite beams with partial shear connection. The former approach uses equilibrium equations and, considering the maximum force that can be transferred by the shear connection, determines the position of neutral axis within the cross-section and hence the plastic moment resistance, while the interpolation method simply adopts a linear interpolation

Table 4
Concrete slab dimensions and material properties for parametric studies.

b_{eff} (mm)	h_c (mm)	f_y (N/mm^2)	f_u (N/mm^2)	f_{cm} (N/mm^2)
1500	120	275	390	30
1500	120	355	490	35
1500	120	420	520	35
1500	150	460	540	40

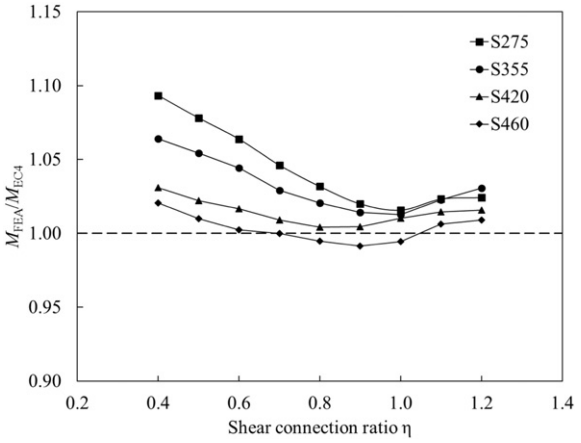

Fig. 9. Comparison of bending strength of composite beams from FE model and EC4.

between the plastic moment resistance of the bare steel section for $\eta = 0$ and the full plastic moment resistance of the composite beam for $\eta = 1$. Fig. 9 shows a comparison of the maximum moment capacity (M_{FEA}) of the 36 beams obtained from the FE model with the results (M_{EC4}) determined using the Eurocode 4 equilibrium method.

It can be seen that, for composite beams with partial shear connection, the ratio of M_{FEA}/M_{EC4} decreases with an increase of the degree of shear connection and the grade. The equilibrium method predicts accurate results when $\eta > 0.8$, and conservative ones when $\eta < 0.8$. However, the equilibrium method may overestimate the bending capacity of composite beams with high strength steel (S460) because the assumed rigid plastic model overestimates the development of plasticity.

On the basis of the numerical results generated, a tentative approach to calculate the bending capacity of composite beams with partial shear connection, but accounting for strain hardening, is proposed. The adopted approach utilizes the CSM bending resistance of the bare steel section M_{csm} described in Section 2 for $\eta = 0$ and the proposed bending resistance for the composite beams with full shear connection $M_{csm,c}$ derived in Section 3.2 for $\eta = 1$, in conjunction with an interpolation function for intermediate degrees of shear connection. In Fig. 10, the ratio between M_{FEA} and $M_{csm,c}$ is plotted on the vertical axis and the degree of shear connection η is given on the horizontal axis. It can be seen that the composite beams with conventional mild steel ($f_y < 460$ MPa) exhibit a similar linear trend between $\eta = 0.4$ and $\eta = 1$, indicating that a bi-linear interpolation function may be used to predict the ultimate capacity of composite beams with partial shear connection allowing for strain hardening, as shown in Fig. 10, where an indicative interpolation line is presented. For composite beams with high strength steel, lower reduction factors may be needed. Clearly a wide range of

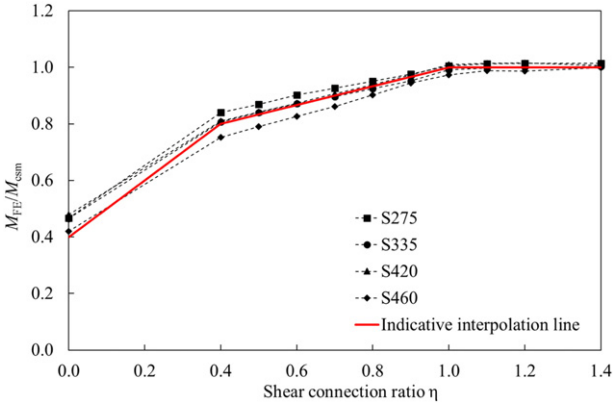

Fig. 10. Indicative interpolation function for composite beams with partial shear connection.

parameters including different cross-sectional geometries, reinforcement ratios and steel grades need to be considered before the method is suitable for use in practical design; the present study demonstrates the validity of the proposed approach.

4. Conclusions

Developments to the Continuous Strength Method (CSM) for hot-rolled carbon steel, covering recent refinements, have been described. A quad-linear material model, enabling representation of both the yield plateau and strain hardening, has been proposed and used for the derivation of CSM resistance equations for the compression and bending of hot-rolled carbon steel members. Test data on hot-rolled carbon steel stub columns and beams were used to make comparisons with the CSM and EN 1993-1-1 design provisions. It was shown that the CSM offers improved mean resistance predictions and lower scatter compared with EN 1993-1-1. The method was then extended to composite beams under sagging bending moment, where the influence of strain hardening has been found previously to be significant. For composite beams with full shear connection, a new analytical model has been developed accounting for strain hardening through the proposed material model, and explicit resistance functions have been derived. Comparison of the predictions with 14 test results on composite beams from the literature showed that the proposed analytical equations may be more accurate than the current codified approaches. A two-dimensional FE model was then developed and validated against test results reported in existing studies. Based on subsequently generated numerical parametric results, a new design approach was outlined for composite beams with partial shear connection. Additional analyses considering various geometric properties and different reinforcement ratios for composite beams are needed to confirm the wider applicability of the proposed design method to steel-concrete composite beams.

Acknowledgements

The financial support provided by the China Scholarship Council (CSC) for the second author's PhD study at Imperial College London is acknowledged.

References

[1] Gardner L, Saari N, Wang F. Comparative experimental study of hot-rolled and cold-formed rectangular hollow sections. Thin-Walled Struct 2010;48(7):495–507.
[2] Liew A, Boissonnade N, Gardner L, Nseir J. Experimental study of hot-rolled rectangular hollow sections. Proceedings of the Annual Stability Conference, Structural Stability Research Council; 25–28 March 2014 (Toronto, Canada).
[3] Byfield MP, Nethercot DA. An analysis of the true bending strength of steel beams. Proc Inst Civ Eng Struct Build 1998;128:188–97.
[4] Ansoutian P. Plastic rotation of composite beams. J Struct Div ASCE 1982;108(3):643–59.
[5] Chapman J, Balakrishnan S. Experiments on composite beams. Struct Eng 1964;42(11):369–83.
[6] Chung KF, Chan C. A numerical investigation into the effect of strain hardening on the structural behaviour of simply supported composite beams. Proceedings of the 9th Pacific Structural Steel Conference; 19–22 October 2010. p. 988–93 (Beijing, China).
[7] Gardner L, Nethercot DA. Stainless steel structural design: a new approach. Struct Eng 2004;82(21):21–8.
[8] Ashraf M, Gardner L, Nethercot DA. Structural stainless steel design: resistance based on deformation capacity. J Struct Eng ASCE 2008;134(3):402–11.
[9] Afshan S, Gardner L. The continuous strength method for structural stainless steel design. Thin-Walled Struct 2013;68:42–9.
[10] Gardner L. The continuous strength method. Proc Inst Civ Eng Struct Build 2008;161(3):127–33.
[11] Gardner L, Wang FC, Liew A. Influence of strain hardening on the behaviour and design of steel structures. Int J Struct Stab Dyn 2011;11(5):855–75.
[12] Liew A, Gardner L. Ultimate capacity of structural steel cross-sections under compression, bending and combined loading. Structure 2015;1:2–11.
[13] Su MN, Young B, Gardner L. Testing and design of aluminium alloy cross-sections in compression. J Struct Eng ASCE 2014;140(9):04014047.
[14] Schafer BW, Ádány S. Buckling analysis of cold-formed steel members using CUFSM: conventional and constrained finite strip methods. Proceedings of the 18th International Specialty Conference on Cold-Formed Steel Structures; 26–27 October 2006. p. 39–54 (Orlando, Florida, USA).
[15] Seif M, Schafer BW. Local buckling of structural steel shapes. J Constr Steel Res 2010;66(10):1232–47.
[16] EN 1993-1-5. Eurocode 3: Design of Steel Structures — Part 1–5: Plated Structural Elements. European Committee for Standardization (CEN), Brussels; 2006.
[17] Schafer BW. Review: the direct strength method of cold-formed steel member design. J Constr Steel Res 2008;64(7):766–78.
[18] EN 1993-1-1. Eurocode 3: Design of Steel Structures — Part 1–1: General Rules and Rules for Buildings. European Committee for Standardization (CEN), Brussels; 2005.
[19] Wang F. A Deformation Based Approach to Structural Steel Design. (PhD thesis) London, UK: Imperial College London; 2011.
[20] Sadowski AJ, Rotter JM, Reinke T, Ummenhofer T. Statistical analysis of the material properties of selected structural carbon steels. Struct Saf 2015;53:26–35.
[21] Chan TM, Gardner L. Bending strength of hot-rolled elliptical hollow sections. J Constr Steel Res 2008;64:971–86.
[22] Kuhlmann U. Definition of flange slenderness limits on the basis of rotation capacity values. J Constr Steel Res 1989;14:21–40.
[23] Wang J, Afshan S, Gkantou M, Theofanous M, Baniotopoulos C, Gardner L. Flexural behaviour of hot-finished high strength steel square and rectangular hollow sections. J Constr Steel Res 2016;121:97–109.
[24] Shi G, Ban H, Bijlaard FS. Tests and numerical study of ultra-high strength steel columns with end restraints. J Constr Steel Res 2012;70:236–47.
[25] Foster A, Gardner L. Ultimate behaviour of steel beams with discrete lateral restraints. Thin-Walled Struct 2013;72:88–101.
[26] D'Aniello M, Landolfo R, Piluso V, Rizzano G. Ultimate behaviour of steel beams under non-uniform bending. J Constr Steel Res 2012;78:144–58.
[27] Cuk P, Rogers D, Trahair N. Inelastic buckling of continuous steel beam-columns. J Constr Steel Res 1986;6:21–52.
[28] Wilkinson TJ. The Plastic Behaviour of Cold-formed Rectangular Hollow Sections. (PhD thesis) Sydney, Australia: The University of Sydney; 1999.
[29] Saloumi E, Hayeck M, Nseir J, Boissonnade N. Experimental characterization of the rotational capacity of hollow structural shapes. Proceedings of the 15th International Symposium on Tubular Structures; 27–29 May 2015. p. 591–4 (Brazil).
[30] Shokouhian M, Shi Y. Flexural strength of hybrid steel I-beams based on slenderness. Eng Struct 2015;93:114–28.
[31] Nseir J. Development of a New Design Method for the Cross-section Capacity of Steel Hollow Sections. (PhD thesis) Liège, Belgique: Université de Liège; 2015.
[32] Sawyer HA. Post-elastic behaviour of wide-flange steel beams. J Struct Div ASCE 1961;87(8):43–71.
[33] Lukey AF, Adams PF. Rotation capacity of wide-flange beams under moment gradient. J Struct Div ASCE 1969;95(6):1173–88.
[34] Roik K, Kuhlmann U. Experimentelle ermittlung der rotationskapazität biegebeanspruchter I-profile (Teil 2), Der Stahlbau (56), Heft, 12; 1987[in German].
[35] Chr P. Berjcht über versuche zur rotationskapazität von walzprofilen in fließgelenken und folgerungen für die fließzonenund fileßgelenktheorie. Fachhochschule Münster: Stahlbau seminar; 1988[in German].
[36] EN 1994-1-1. Eurocode 4: Design of Composite Steel and Concrete Structures — Part 1–1: General Rules and Rules for Buildings. Brussels: European Committee for Standardization (CEN); 2005.
[37] Johnson R, Molenstra N. Partial shear connection in composite beams for buildings. P I Civil Eng Pt 2 1991;91(1):670–704.
[38] Kucukler M. Influence of Strain Hardening on Sagging Bending Moment Resistance of Composite Beams With Full or Partial Shear Connections. (MSc thesis) London, UK: Imperial College London; 2011.
[39] Abaqus. Reference Manual, Version 6.11. France: Simulia, Dassault Systèmes; 2011.
[40] Gattesco N. Analytical modelling of nonlinear behaviour of composite beams with deformable connection. J Constr Steel Res 1999;52(2):195–218.
[41] Zona A, Ranzi G. Finite element models for nonlinear analysis of steel-concrete composite beams with partial interaction in combined bending and shear. Finite Elem Anal Des 2011;47(2):98–118.
[42] Queiroz FD, Queiroz G, Nethercot DA. Two-dimensional FE model for evaluation of composite beams, I: formulation and validation. J Constr Steel Res 2009;65(5):1055–62.
[43] Ban H, Bradford M. Flexural behaviour of composite beams with high strength steel. Eng Struct 2013;56:1130–41.
[44] EN 1992-1-1. Eurocode 2: Design of Concrete Structures — Part 1–1: General Rules and Rules for Buildings. Brussels: European Committee for Standardization (CEN); 2004.
[45] Vasdravellis G, Uy B, Tan EL, Kirkland B. Behaviour and design of composite beams subjected to sagging bending and axial compression. J Constr Steel Res 2015;110:29–39.
[46] Kwon G, Engelhardt MD, Klinger RE. Experimental behaviour of bridge beams retrofitted with post-installed shear connectors. J Bridge Eng ASCE 2011;16:536–45.
[47] Loh HY, Uy B, Bradford M. The effects of partial shear connection in the hogging moment regions of composite beams, part I-experimental study. J Constr Steel Res 2004;60:897–919.